Methods of Electron Structure Spectroscopy in Molecular Organic Solids Based on Transient Photoconductivity with Space Charge

R. HANDLÍŘ, M. WEITER, and F. SCHAUER

Faculty of Chemistry, Technical University, CZ-637 00 Brno

Received 18 April 1996

Space-charge-limited currents (SCLC) in both steady-state (S-SCLC) and transient (T-SCLC) regimes may be with advantage used as tools for the study of the density of localized states (DOS) in organic molecular semiconductors. The only prerequisite for the experimental observation of SCLC is a reasonably long Maxwell relaxation time, SCLC are readily observed in high resistivity materials with mobile carriers.

This paper presents the new possibilities of the T-SCLC method for elucidation of the DOS in organic molecular solids with practical examples of modelling, reconstruction of post-transit data and its application for amorphous hydrogenated silicon and poly(methylphenylsilylene).

Space-charge-limited currents (SCLC), both in transient regimes (T-SCLC) and steady state (S-SCLC) in organic semiconductors may potentially help to study the new models, faced by the branch of organic semiconductors. Also, from the applicational point of view, the metastability and resulting degradation starts to be a major topic.

Transient SCLC method [1] is a powerful method due to the extra time variable, even if experimentally very sophisticated. Information may be drawn from both pulse-light generated transients [2] and from transients due to voltage steps [3].

In this paper, devoted to T-SCLC, a method is presented for the elucidation of the density of localized states (DOS) and recombination mechanisms operative in material examined.

Physical Background

For the purpose of the physical insight into SCLC, let us bring first the basic ideas within an oversimplified mathematical framework, elaborating it further. Let us consider a plane-parallel homogeneous (as to the DOS and the mobility) sample. The crucial condition for the SCLC to occur is the existence of the charge reservoir at $x = 0$ and an extracting counter electrode at $x = L$. On the application of the external voltage, two competing processes occur: **first** — the electric field starts to move the mobile carriers from the reservoir with a time-dependent velocity $\langle v(t) \rangle$ and thus with time-dependent drift mobility $\mu(t)$ defined $\langle v(t) \rangle = \mu(t)F$ [4], where $F = U/L$ is the electric field strength and U is the applied voltage. The movement of the carriers is a complex process, resulting from both the trapping in *all the available states* and retrapping from those, being in *quasi-equilibrium with the transport band.* So, the transit time of the carriers across the sample t_t is not a straightforward quantity [4], but for the purpose of the present explanation we consider it as a measurable and meaningful observable, giving the drift mobility

$$\mu_d = \frac{L}{Ft_t} = \frac{L^2}{Ut_t} \tag{1}$$

It should be stressed that the drift mobility is not a material constant, but severely depends on the **deepest states being in quasi-equilibrium** with the carriers in the transport band at the transit time, depending in turn on the time itself and the temperature.

Secondly a parallel and competing process is the charge neutralization in the sample, expressed by the Maxwell relaxation time, depending in the first order on the instantaneous sample conductivity $\sigma(t) = en_f(t)\ \mu_0 = e(n_f + n_t)\ \mu_d$

$$t^M(t) = \frac{\varepsilon\varepsilon_0}{\sigma} = \frac{\varepsilon\varepsilon_0\Theta}{en_f\mu_d} \tag{2}$$

where $\Theta = n_f/n_s$, $n_s = n_f + n_t$, n_f is the concentration of free and n_t trapped carriers, respectively, and μ_0 is the mobility of the carriers in the transport band. The time as a variable enters eqn (2) as a result of the time evolution of the conductivity.

Basically, depending on the relation of the transit time t_t and the Maxwell relaxation time t^M, three regimes of transport, summarized in the table, may be observed.

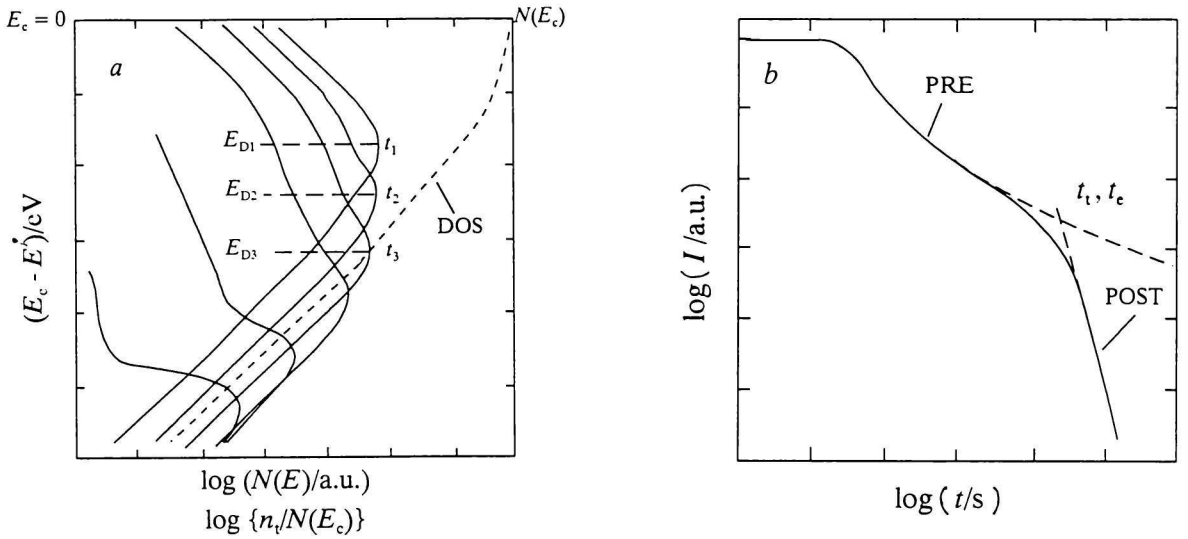

Fig. 1. *a*) The artificial DOS with the time-dependent position of the thermalization energy E_D and the time evolution of the DOS occupation. *b*) The current—time I—t dependence with the corresponding pre- (PRE) and post-extraction (POST) time dependences denoted.

1	$t^M < t_t$	no space charge low or high field transport (standard charge transport)
2	$t^M > t_t$	space charge exists nonsteady state T-SCLC
3	$t^M = t_t$	space charge exists steady state S-SCLC

The case 2 is distinctive for all nonsteady-state transient phenomena, where space charge exists, namely time of flight (TOF) and T-SCLC. The current density is principally governed by $\Theta(t)$ but now the function $\Theta(t)$ is time-dependent, giving

$$I_{SCLC}(t) = \frac{\varepsilon\varepsilon_0\mu_0\Theta(t)U^2}{L^3} \qquad (3)$$

till the extraction time

$$t_e = \frac{Q}{I_{SCLC}} = \frac{Q}{\text{const } S\varepsilon\varepsilon_0\mu_D\dfrac{U^2}{d^3}} \qquad (4)$$

where Q is the charge, available at the injecting contact (*e.g.* optically generated), S is the sample area and const is near to 1.

In order to explain the T-SCLC method, we depicted schematically in Fig. 1*a* the artificial DOS with several positions of the thermalization energy level E_D (eqn (5)) dividing the states that are in quasi-equilibrium with the transport band and those, that are not, and in Fig. 1*b* the corresponding current—time I—t dependence. The main idea of the T-SCLC method as a spectroscopic method is very simple: starting at $t = 0$, all the states up to the Fermi level start to trap carriers. Subsequently, the shallowest carriers start to equilibrate with the transport band, allowing us to formulate $\Theta(t)$ function in eqn (3). The equilibration process is complete above the thermalization energy defined [5]

$$E_D(t) = kT\ln(\nu t) \qquad (5)$$

where ν is the attempt-to-escape frequency ($\nu = 10^{12}$ s^{-1}). Even if challenged for some DOS [5], this formula for the evolution of the distribution function $\Theta(t)$ is very often used in amorphous semiconductors, where the broad DOS is encountered [6]. So, as the time proceeds, the deeper and deeper states are included in the thermalization process (Fig. 1*a*). Then the corresponding DOS value is reflected in the resulting $I(t)$ characteristics but not in a very straightforward manner.

The termination of the just described transient may be the result of the *injecting contact to fail to replenish the carriers* either due to its inferior properties [3] or finite capacity of the optically generated reservoir [2], the so-called *extraction time* t_e, defined by eqn (4) (and more precisely in [7]).

After extraction time, another possibility for DOS evaluation from $I(t)$ SCLC transients, using the *post-transit analysis* (the idea is also depicted in Fig. 1), has been suggested in [8]. After the exhaustion of the contact reservoir, the carriers, trapped in the traps start to be emitted to the transport band and are instantaneously swept from the sample, forming the post-extraction current. The process of the emission from the traps starts from the states corresponding to extraction time t_e and continues to deeper states as the time proceeds according to eqn (5).

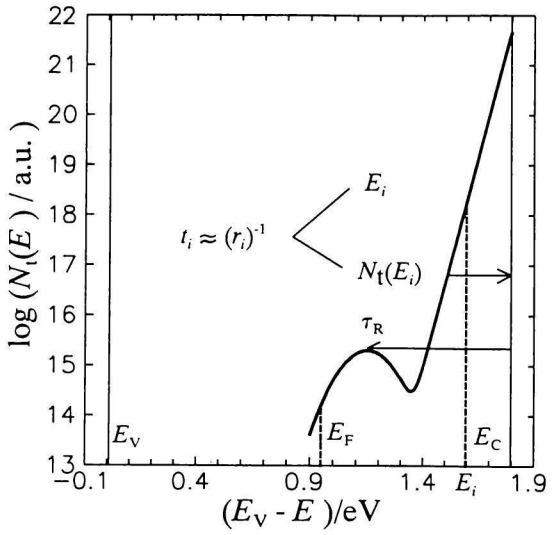

Fig. 2. Electron transitions in the time domain photoconductivity spectroscopies.

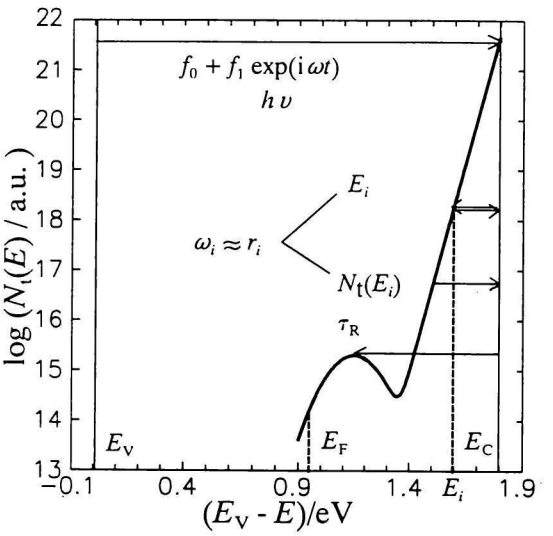

Fig. 3. Electron transitions in the frequency domain photoconductivity spectroscopies.

THEORETICAL

In Figs. 2 and 3 the electron transitions in both the time (Fig. 2) and frequency (Fig. 3) domain are shown. We want to show that the measurements in the time domain correspond to any transient photoconductivity measurements (including time of flight and T-SCLC) and the measurements in the frequency domain correspond to phase-sensitive photoconductivity (PSP). Both types of measurements are complemental and transferable using the Fourier transform.

Theory of Evaluation in the Time Domain

Post-extraction transient space-charge-limited currents (T-SCLC) can in principle provide a very wide time span of data (from about 10^{-8} to 10^2 s) that can provide information about the DOS. These data can be evaluated using the standard small-signal post-transit analysis introduced in [8]

$$N_t(E) = 2tI(t)/Q_0 t_0 \nu \tag{6}$$

$$E_D(t) = \boldsymbol{k}T \ln(\nu t) \tag{7}$$

where $N_t(E)$ is the sought density of states (DOS) distribution, t is the time, E_D the thermalization energy, $I(t)$ the current at the time t, Q_0 the total collected charge, and t_0 the transit time.

Theory of Evaluation in the Frequency Domain

Following equations represent the rates of generation, capture, release, and recombination of the mobile and of the trapped electrons after the light generation with the harmonic modulated intensity with the frequency ω [9]

$$\frac{dn(E)}{dt} = f_0 + f_1 e^{i\omega t} - \int_{E_c}^{E_d} \frac{dn_t(E)}{dt} - \frac{n - n_d}{\tau_R} \tag{8}$$

where

$$\frac{dn_t(E)}{dt} = nV\sigma[N_t(E) - n_t(E)] - N_c V \sigma n_t(E) e^{-\frac{E_c - E}{kT}} \tag{9}$$

and

$$E_d = E_{Fn} + \boldsymbol{k}T \ln \frac{\sigma_n n}{\sigma_p p} \tag{10}$$

where n (p) is the concentration of mobile electrons (holes), n_t the concentration of trapped electrons, n_d the dark concentration of electrons, E_d the electron demarcation level, V the electron thermal velocity, σ_n (σ_p) are the electron (hole) capture cross-sections (next we use only σ for electrons), and N_c is the effective density of states in the conduction band.

As the light is harmonically modulated, solution of equations can be obtained in the form of small harmonic perturbation [9]

$$n = n_0 + \hat{n}_1 e^{i\omega t} \tag{11}$$

with

$$\hat{n}_1 = \frac{f_1}{(A^2 + B^2)^{1/2}} e^{-i\phi} \tag{12}$$

and

$$\tan \phi(\omega) = \frac{B}{A} \tag{13}$$

where

$$A = \frac{1}{\tau_R} + \int_{E_c}^{E_d} G_2(E) V \sigma N_t(E) dE \tag{14}$$

and

$$B = \omega + \frac{1}{2} \int_{E_c}^{E_d} G_1(E) V \sigma N_t(E) dE \tag{15}$$

The G_1 and G_2 are the so-called weighting functions

$$G_1(E) = \frac{2D\exp((E_{Fn}-E)/\boldsymbol{k}T}{D^2+[1+\exp((E_{Fn}-E)/\boldsymbol{k}T)]^2} \quad (16)$$

and

$$G_2(E) = D^2\exp((E_{Fn}-E)/\boldsymbol{k}T)/ \\ /\{[1+\exp((E_{Fn}-E)/\boldsymbol{k}T)] \\ [D^2+\{1+\exp((E_{Fn}-E)/\boldsymbol{k}T)\}^2]\} \quad (17)$$

$$D = \frac{\omega}{N_c V\sigma\exp((E_{Fn}-E)/\boldsymbol{k}T)} \quad (18)$$

where D represents the ratio of modulation frequency to the thermal emission rate of trapped electrons at the quasi-Fermi level. When $D \gg 1$ the E_ω is defined as maximum of $G_1(E)$

$$E_\omega = \boldsymbol{k}T\ln\left(\frac{N_c V\sigma}{\omega}\right) = \boldsymbol{k}T\ln\left(\frac{\nu}{\omega}\right) \quad (19)$$

To obtain $N_t(E)$ we must know $\hat{n}_1$ (eqn (12)). It is clear that

$$I_1 = |\hat{I}_1| = \mu_0 eFS|\hat{n}_1| \quad (20)$$

where I_1 is the measured modulated photocurrent, μ the mobility of electrons, e the electron charge, F field strength, and S is the cross-section of the sample.

Then from eqn (13) it is

$$\cos\phi = \frac{A}{(A^2+B^2)^{1/2}} \quad (21)$$

$$\sin\phi = \frac{B}{(A^2+B^2)^{1/2}} \quad (22)$$

Using eqns (14), (17), (20), (21), and (15), (16), (20), (22) we obtain

$$\frac{1}{\tau_R} + \int_{E_c}^{E_d} G_2(E)V\sigma N_t(E)\mathrm{d}E = \frac{\mu_0 ef_1 FS\cos\phi(\omega)}{I_1(\omega)} \quad (23)$$

and

$$\omega + \frac{1}{2}\int_{E_c}^{E_d} G_1(E)V\sigma N_t(E)\mathrm{d}E = \frac{\mu_0 ef_1 FS\sin\phi(\omega)}{I_1(\omega)} \quad (24)$$

From both eqns (23) and (24) the density of electron states $N_t(E)$ can be in principle obtained. Unfortunately the integration of both eqns (23) and (24) is intractable. Some simplification must be used. Most of authors [9—14] use eqn (24) (the so-called imaginary term). The function $G_1(E)$ has the maximum at E_ω (Fig. 4). This function is usually approximated by the δ-function and then eqn (24) can be approximately expressed as

$$\omega + \frac{1}{2}C_1\boldsymbol{k}TV\sigma N_t(E_\omega) = \frac{\mu_0 ef_1 FS\sin\phi(\omega)}{I_1(\omega)} \quad (25)$$

and the density of states is then (when $C_1 \approx \pi$ [9])

$$N_t(E) = \frac{2}{\pi\sigma V\boldsymbol{k}T}\left[\frac{\mu_0 ef_1 F\sin(\phi(\omega))}{I_1(\omega)} - \omega\right] \quad (26)$$

But the approximation of $G_1(E)$ by the δ-function is not so perfect because the function $G_1(E)$ is quite wide (Fig. 4).

To obtain the density of states we can also use the real term, eqn (23) [14, 15].

If eqn (23) is differentiated over $\ln(\omega)$ and τ_R is considered to be constant with the frequency, then the expression can be rewritten

$$\int_{E_c}^{E_d} g_2(E)V\sigma N_t(E)\,\mathrm{d}E = \\ = \mu_0 ef_1 FS\frac{\partial}{\partial\ln(\omega)}\left[\frac{\cos\phi(\omega)}{I_1(\omega)}\right] \quad (27)$$

with

$$g_2(E) = \frac{\partial G_2(E(\omega))}{\partial\ln(\omega)} \quad (28)$$

Function G_2 was defined by eqn (17). The plot of this function (G_2) and its derivative (g_2) is in Fig. 4. In Fig. 5 is the comparison of the function G_1 and g_2. It seems that g_2 is narrower than G_1 at the energy E_ω, so the δ-approximation is more appropriate. The problem rests in the existence of two peaks in the function g_2 (the first is situated at E_ω and the second at the quasi-Fermi level E_{Fn} (Fig. 4)), with the necessity of separate integration for both of them. Approximate solution is

$$C_{21}\boldsymbol{k}TV\sigma N_t(E_\omega) - \frac{1}{2}C_{22}\boldsymbol{k}TV\sigma N(E_{Fn}) = \\ = \mu_0 ef_1 FS\frac{\partial}{\partial\ln(\omega)}\left[\frac{\cos\phi(\omega)}{I_1(\omega)}\right] \quad (29)$$

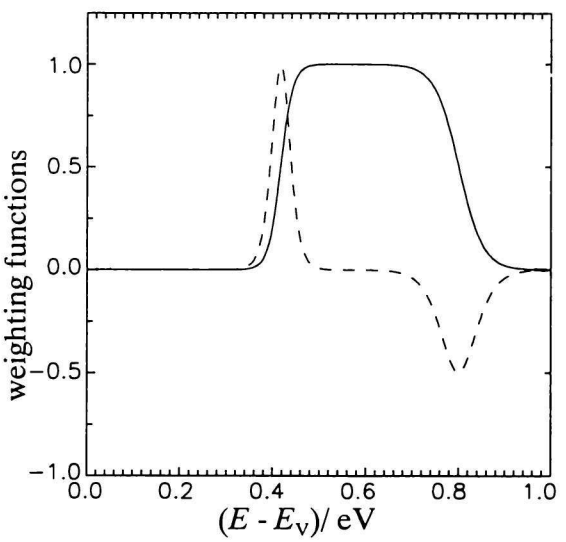

Fig. 4. The weighting function $G_2(E)$ (——) and its derivative with respect to $\ln(\omega)$ $g_2(E)$ (– – –) for $\omega = 10^5$ s^{-1}.

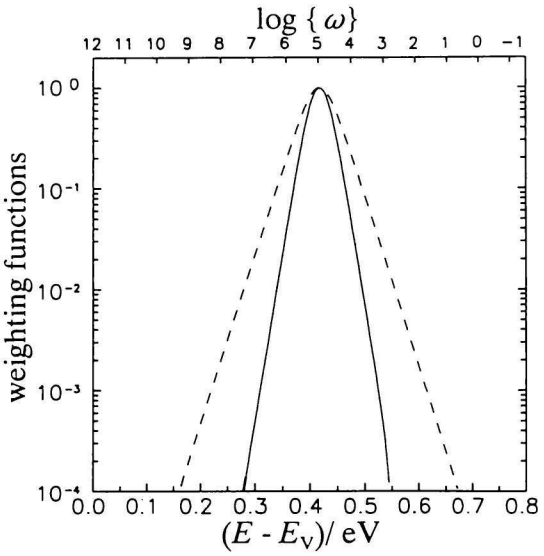

Fig. 5. The weighting functions $G_1(E)$ (– – –) and $g_2(E)$ (——) for $\omega = 10^5$ s^{-1}.

and then supposing $C_{21} \approx C_{22} \approx C_2$

$$N_t(E_\omega) = \frac{\mu_0 e f_1 F S}{kTV\sigma C_2} \frac{\partial}{\partial \ln(\omega)} \left[\frac{\cos\phi(\omega)}{I_1(\omega)}\right] + \frac{1}{2} N_t(E_{Fn}) \qquad (30)$$

This expression can be used with advantage for the evaluation of the density of states above the quasi-Fermi level with superior results compared to eqn (*26*).

EXPERIMENTAL

To test our ideas, we started first with the transform of model data. The procedure was following. First, the model data in the time domain $I(t)$ were used and transformed to the frequency domain, and only then we attempted the reconstruction of the DOS function using eqn (*30*). We found this procedure very noise-suppressing, which is an inherent property of any integral transform. For the transformation of the transient current $I(t)$ to the frequency domain $I(\omega)$ we used the standard Fourier transform [10, 11]

$$\hat{I}(\omega) = \int I(t) e^{-i\omega t} dt = |I_{ac}(\omega)| e^{i\phi(\omega)} \qquad (31)$$

To test our numerical Fourier transform (*31*) and the evaluation of transient photoconductivity data (using eqns (*14*) and (*30*)) we tested the model data of transient photoconductivity (Fig. 6) [16]. The model input data are in Fig. 6. For the reconstruction of DOS from TPC data we used eqn (*31*) to transform the data to the frequency domain and then eqns (*19*) and (*30*) to evaluate the DOS function. The reconstructed DOS functions for $T = 200$ K are in Fig. 7. We can see that our model test calculation gives very satisfactory results.

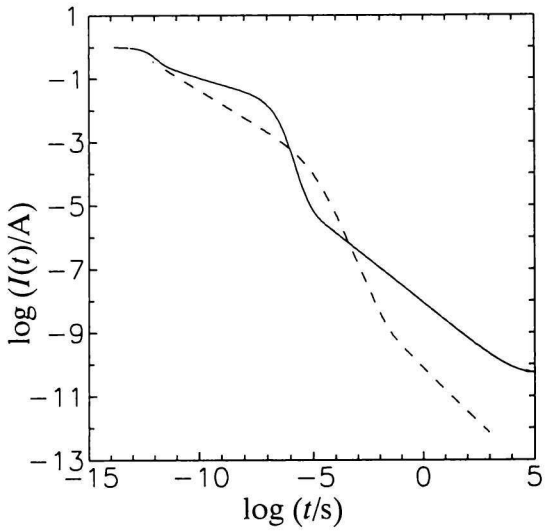

Fig. 6. The model transient photoconductivity data $I(t)$ [16] for the DOS function from Fig. 7 for $T = 200$ K (– – –) and 300 K (——).

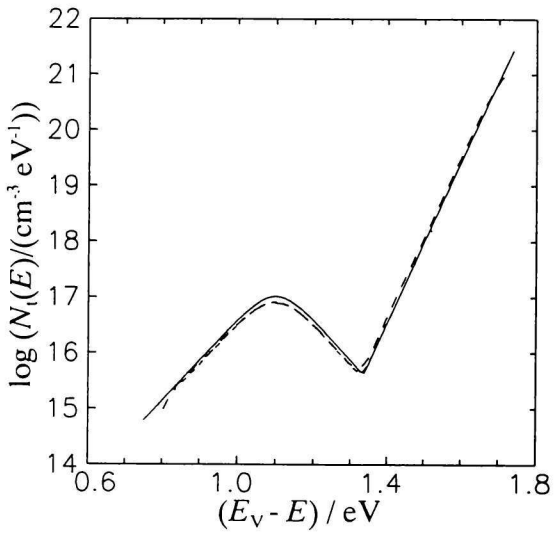

Fig. 7. The reconstructed DOS function using the procedure given in the text (eqns (*19*) and (*30*)) (– – –). The input DOS function used for the model is also given (——).

The real experiments were carried out on two types of materials. First a prototypical material – amorphous hydrogenated silicon (a-Si:H) in device-grade quality was used in p–i–n configuration [17]. Samples were examined in different degraded states, degradation was caused by the current of 300 mA cm^{-2} for 0, 7, 27, and 150 min. Both electron and hole post-transit currents were measured in the time domain. The results of measurements are presented in Figs. 8 and 9 and the reconstruction of DOS functions is in Fig. 10. (More details are given in [18—20].)

The second material measured was poly(methylphenylsilylene). Polysilylenes represent a new class of

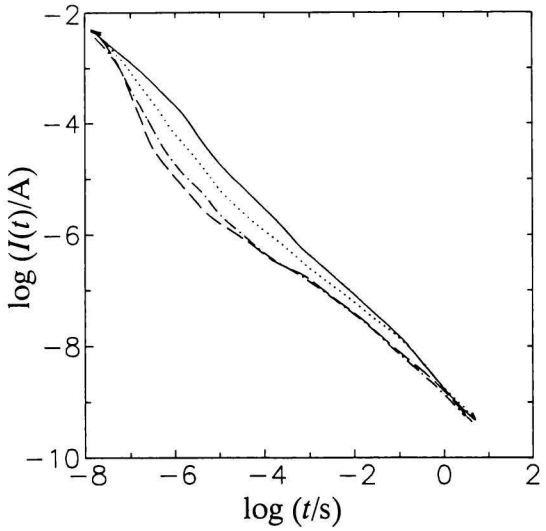

Fig. 8. The post-transit **electron** currents for the a-Si:H p–i–n structure parametric in the different stages of degradation due to the current degradation, soaking current density 300 mA cm^{-2}, soaking time 0 min (——), 7 min (· · ·), 27 min (– · –·), and 150 min (— —).

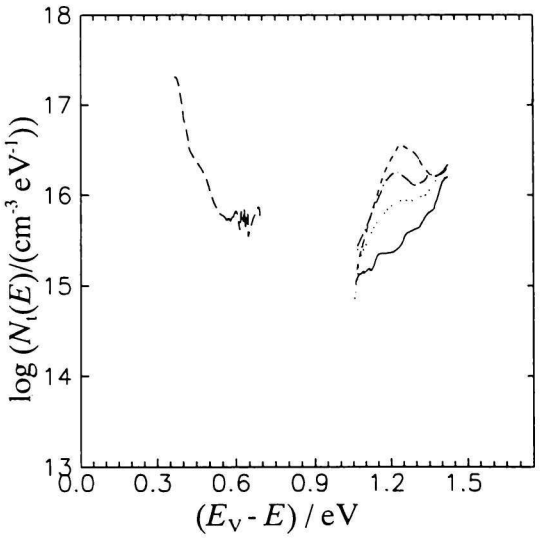

Fig. 10. Reconstruction for the DOS of the $I(t)$ signals for the a-Si:H p–i–n structure from Figs. 8 and 9 using the procedure given in the text (eqns (*19*) and (*30*)). Holes (— —), electrons, soaking time 0 min (——), 7 min (· · ·), 27 min (· – ·–), and 150 min (– – –).

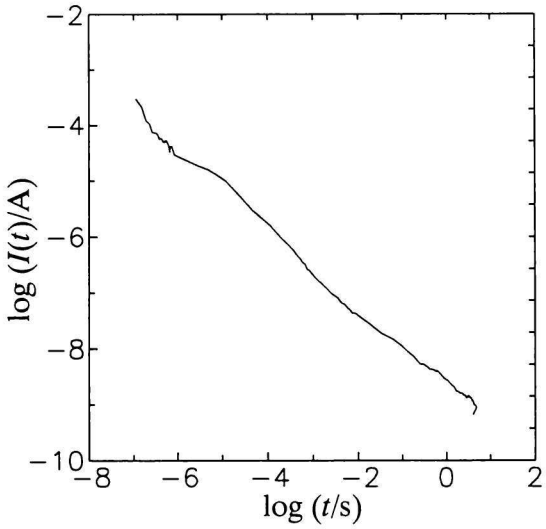

Fig. 9. The post-transit **hole** current for the a-Si:H p–i–n structure identical to Fig. 8.

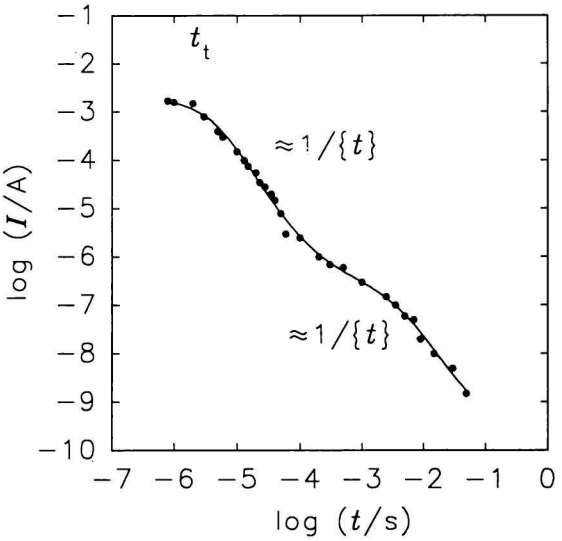

Fig. 11. The post-transit **hole** current for the poly(methylphenylsilylene) structure

polymers of exceptionally high intrinsic hole mobility with comparatively low activation energy due to the σ-conjugation in the main chain, conjugation length being from 10 to 30 [21]. Besides, the transport is observed to be only slightly nondispersive with a weak electrical field dependence and with low trapping effects [22—24]. Though the generally accepted description of the transport in polymers with a high degree of disorder is the hopping *via* transport sites in a disordered solid matrix, surprisingly little is known about the trapping states, their energy distribution and their origin. Polysilylenes, due to their unique properties, thus may serve as a model material for the study of the trapping events in organic solids. The typical post-transit signal for the field strength $F = 1.5 \times 10^6$ V cm^{-1} is in Fig. 11 obtained from several responses with different time windows. Also marked is the corresponding transit time t_t. In Fig. 12 is then the cumulative DOS obtained from the evaluation of hole transients in the framework of the post-transit analysis, giving up-to-now not observed spectrum of electron states.

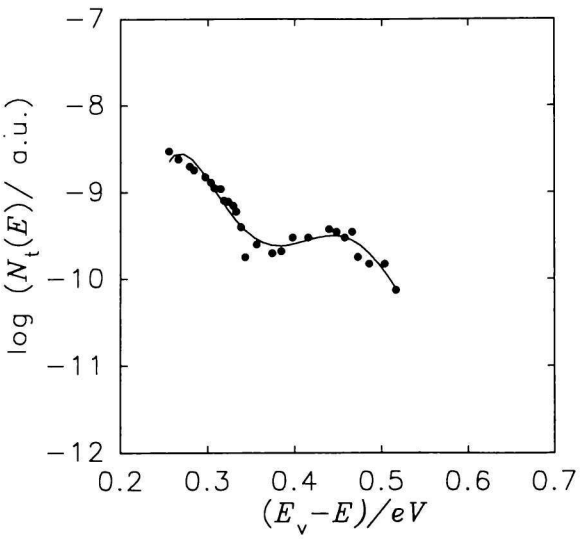

Fig. 12. Reconstruction for the DOS of the $I(t)$ signals for the poly(methylphenylsilylene) structure using the procedure given in the text (eqns (*19*) and (*30*), $\nu = 10^9$ Hz was used).

CONCLUSION

The post-transit analysis in general and in space-charge-limited current mode provides a new and prospective method of elucidation of the DOS in a wide energy range in amorphous and noncrystalline materials, including organic ones.

The framework for evaluation of the post-transit signals is given in both the time and frequency domains. The frequency domain approach, due to the Fourier transform used, is much less noise susceptible.

The measurements of both amorphous hydrogenated silicon and a polysilylene gave very satisfactory results. For a-Si:H the applicability of the method for the study of the degradation on both the electron and hole trapping states was demonstrated. The measurements on the typical conjugated silicon backbone polymer, poly(methylphenylsilylene) showed the DOS distribution in this perspective material.

REFERENCES

1. Lampert, M. A. and Mark, P., *Current Injection in Solids.* Academic Press, New York, 1970 and Kao, K. C. and Hwang, W., *Electrical Transport in Solids.* Pergamon Press, Oxford, 1981.
2. Kočka, J., in *Proc. of the 7th Int. School on Cond. Matter Phys.*, p. 129. Varna, World Scientific Publ. Co., Singapore, 1989.
3. Snow, E. and Silver, M., *J. Non-Cryst. Solids 77 & 78,* 451 (1985).
4. Schiff, E. A. and Silver, M., in *Amorphous Silicon and Related Materials,* p. 825. World Scientific Publ. Co., Singapore, 1989.
5. Pollak, M., *Phil. Mag. 36,* 1157 (1977).
6. Marshall, J. M., in *Amorphous Silicon and Related Materials,* p. 799. World Scientific Publ. Co., Singapore, 1989.
7. Juška, G. M., Viliunas, M., Klíma, O., Šípek, E., and Kočka, J., *Phil. Mag. B69,* 277 (1994).
8. Seynhaeve, G. F., Barclay, R. P., Adriaenssens, G. J., and Marshall, J. M., *Phys. Rev. B49,* 10196 (1989).
9. Hidetoshi Oheda, J. *Appl. Phys. 52,* 6693 (1981).
10. Main, C., Brüggemann, R., Webb, D. P., and Reynolds, S., *Solid State Commun. 83,* 401 (1992).
11. Main, C., Brüggemann, R., Webb, D. P., and Reynolds, S., *J. Non-Cryst. Solids 164—166,* 481 (1993).
12. Longeaud, C. and Kleider, J. P., *Phys. Rev. B48,* 8715 (1993).
13. Main, C., Brüggemann, R., Webb, D. P., and Reynolds, S., *Phil. Mag. B,* 29 (1990).
14. Lecture of Dr. C. Main on the Chelsea meeting 1994 and ISCMP VARNA '94, September, 1994.
15. Hattori, K., Niwano, Y., Okamoto, H., and Hamakawa, Y., *J. Non-Cryst. Solids 137 & 138,* 363 (1991).
16. The model data were kindly provided by Dr. C. Main from the Dundee Institute of Technology.
17. The post-transit signals were measured on the solar cells provided by Dr. R. E. I. Schropp from the Utrecht University.
18. Schauer, F., Nesládek, M., and Stuchlík, J., *Phil. Mag. Lett. 64,* 321 (1991).
19. Schauer, F., Eliat, A., Nesládek, M., and Adriaenssens, G. J., *Appl. Phys. Lett. 64,* 3009 (1994).
20. Schauer, F., Eliat, A., Nesládek, M., Adriaenssens, G. J., and Stals, L. M., *Mat. Res. Soc. Proc. 336,* 443 (1994).
21. Abkowitz, M. A. and Stolka, M., in *Polymers for Advanced Technologies.* (Lewin, M,, Editor.) P. 225. VCH, New York, 1988.
22. Haarer, D., in *Frontiers of Polymer Research.* (Prasad, P. N. and Nigam, J. K., Editors.) P. 297. Plenum Press, New York, 1991.
23. Kenji Yokoyama and Masaaki Yokoyama, *Solid State Commun. 73,* 199 (1990).
24. Hiroyuki Suzuki, Meyer, H., Simmerer, J., Jiping Yang, and Haarer, D., *Adv. Materials 5,* 743 (1993).

Translated by F. Schauer